HYDROLOGICAL PROCESSES
Hydrol. Process. **17**, 537–557 (2003)
Published online 13 November 2002 in Wiley InterScience (www.interscience.wiley.com). DOI: 10.1002/hyp.1113

Optimal use of high-resolution topographic data in flood inundation models

P. D. Bates,[1]* K. J. Marks[1] and M. S. Horritt[2]

[1] *School of Geographical Sciences, University of Bristol, University Road, Bristol BS8 1SS, UK*
[2] *School of Geography, University of Leeds, Woodhouse Lane, Leeds LS2 9JT, UK*

Abstract:

In this paper we explore the optimum assimilation of high-resolution data into numerical models using the example of topographic data provision for flood inundation simulation. First, we explore problems with current assimilation methods in which numerical grids are generated independent of topography. These include possible loss of significant length scales of topographic information, poor representation of the original surface and data redundancy. These are resolved through the development of a processing chain consisting of: (i) assessment of significant length scales of variation in the input data sets; (ii) determination of significant points within the data set; (iii) translation of these into a conforming model discretization that preserves solution quality for a given numerical solver; and (iv) incorporation of otherwise redundant sub-grid data into the model in a computationally efficient manner. This processing chain is used to develop an optimal finite element discretization for a 12 km reach of the River Stour in Dorset, UK, for which a high-resolution topographic data set derived from airborne laser altimetry (LiDAR) was available. For this reach, three simulations of a 1 in 4 year flood event were conducted: a control simulation with a mesh developed independent of topography, a simulation with a topographically optimum mesh, and a further simulation with the topographically optimum mesh incorporating the sub-grid topographic data within a correction algorithm for dynamic wetting and drying in fixed grid models. The topographically optimum model is shown to represent better the 'raw' topographic data set and that differences between this surface and the control are hydraulically significant. Incorporation of sub-grid topographic data has a less marked impact than getting the explicit hydraulic calculation correct, but still leads to important differences in model behaviour. The paper highlights the need for better validation data capable of discriminating between these competing approaches and begins to indicate what the characteristics of such a data set should be. More generally, the techniques developed here should prove useful for any data set where the resolution exceeds that of the model in which it is to be used. Copyright © 2002 John Wiley & Sons, Ltd.

KEY WORDS LiDAR; geostatistical analysis; inundation prediction; floodplains

INTRODUCTION

High resolution, high accuracy topographic data sets are becoming increasingly available for flood prediction studies in a number of countries. In the UK, for example, a national data collection programme using airborne laser altimetry (LiDAR) and stereo air-photogrammetry is now generating large volumes of high-quality data, and in other countries an increasing number of *ad hoc* surveys are being flown. Previously, flood inundation modelling has been constrained by the limited spatial resolution of available topographic data sources or the cost of acquiring such data through ground survey. Hence, model resolution has typically been much finer than the resolution of the topography data used to drive the simulation. As Blöschl and Grayson (2001: 26–27) note 'it is rare to measure an input or model parameter at the same scale as it is to be used in a model'. Increasing use of the above remote sensing techniques for topographic data capture has largely overcome this problem and caused a rapid shift from a data-poor to a data-rich and spatially complex modelling environment with

* Correspondence to: P. D. Bates, School of Geographical Sciences, University of Bristol, University Road, Bristol BS8 1SS, UK.
E-mail: paul.bates@bristol.ac.uk

Received 20 August 2001
Accepted 11 March 2002

attendant possibilities for model testing and development. Despite an increase in computational power, the relative resolution of model and topography data has now reversed for most codes typically used to simulate flood inundation at the reach scale (see Bates and De Roo (2000) for a review). A newly emergent research area, therefore, is how to integrate such massive data sets with lower-resolution numerical inundation models in an optimum manner that makes maximum use of the information content available. This is the fundamental problem addressed in this paper, and is the direct opposite to that with which most modellers are usually faced. Nevertheless, with the retrieval of further high-resolution data sets from remotely sensed imagery this may become an increasingly common situation in such areas as soil moisture (Franks *et al*., 1998) and snow cover modelling (Cline *et al*., 1998).

In a previous paper (Marks and Bates, 2000) we described the integration of a LiDAR data set with an existing two-dimensional finite element hydraulic model where the mesh discretization was derived independent of the topography. The topography was then assimilated into the model in an *a posteriori* step using weighted nearest-neighbour interpolation to assign an elevation value to each computational node. This is typical of finite element mesh construction in many fields; but this is flawed in a number of ways, which we illustrate below in terms of the specific example of topographic controls on flood inundation prediction.

First, we do not know what are the significant horizontal length scales of topographic variation within the raw data set. Hence, we are unable to establish general guidelines for selection of appropriate model grid resolutions for a given reach. Between closely located points (small horizontal length scales) topographic variations will be indistinguishable from noise (sensor noise, measurement error), and hence are probably unimportant to represent at the model grid scale. Over larger horizontal scales, the difference between topographic points should become more significant, but we are unsure where the cut off between 'noise' and 'significant variation' occurs. We should also distinguish between noise and genuine topographic variations correlated over very small length scales that may be more effectively represented in the friction term. In this respect, there is an analogy between topographic parameterization in hydraulic models and large eddy simulation (LES) of turbulence. In each, grid resolution distinguishes between those flow features at the grid scale or above that need to be captured explicitly, and those at sub-grid scales that are more homogeneous and can be treated statistically in terms of their impact on the mean flow field. A related concept in hydrology, the representative elementary area (REA) of Wood *et al*. (1988), also has an affinity with this idea, although here one selects a grid scale that maximally averages out small-scale variability (Grayson and Blöschl, 2001). The key step in both LES modelling and topographic parameterization is thus to determine the filter width (grid spacing) used to discriminate between flow features that need to be either explicitly or implicitly incorporated into the model. To do this using topography data means we also have to assume that topographic significance is a good proxy measure of hydraulic significance. As flood flows are primarily gravity driven, this is likely to be a reasonable first-order approximation, as suggested in previous modelling studies (e.g. Nicholas and Walling, 1997).

Second, in constructing the mesh *a priori*, and only then interpolating the topographic data onto it (as in Marks and Bates (2000)), we cannot be certain that we have optimally represented the original topographic surface. In assimilating the data into the model it is comprehensively filtered and we have no way of checking that points selected are those that are topographically significant (e.g. break points, linear features, maxima and minima, etc.). For example, Marks and Bates (2000) modelled a 12 km reach of the River Stour, Dorset, UK, using a two-dimensional finite element mesh consisting of 11 265 triangular elements of ~30 m per side and 6049 computational nodes. The LiDAR data set used to parameterize topography at these computational nodes consisted of 261 634 x, y, z co-ordinates with a maximum horizontal spacing of ~4 m. Land surface height at each computational node was assigned on the basis of weighted nearest-neighbour interpolation of the four closest points in the LiDAR data set. Thus, information from only 10·8% of the LiDAR data set was incorporated into the final mesh and the representation of the LiDAR topographic surface by the model may have been less than optimal. We clearly require a method that identifies significant topographic points (whose spacing should be consistent with the general guidelines on filter width identified above) and which then uses

these in the mesh construction process. This should result in an optimum representation of the topographic surface at an appropriate scale.

Third, the River Stour example above demonstrates that whilst we can perhaps develop a methodology for determining those topographic points that should be explicitly incorporated in the model grid, considerable data redundancy is still likely. These data are not, however, information free, and we need to find ways to incorporate this content into the model to make full use of the topographic sources available. As in LES turbulence modelling, relatively homogeneous sub-grid scale features may still have an impact on the mean flow field, and, similarly, a sub-grid closure model is required. Grayson and Blöschl (2001) suggest three increasingly realistic methods of achieving such a closure: by using an 'effective' grid square value for the parameter (see Beven (1989)); by using a distribution function to represent sub-grid variability; or by parameterizing the sub-grid variability directly. Sub-grid topography impacts on hydraulic predictions of inundation extent in a number of ways. For fixed grid (Eulerian) numerical models, sub-grid topography controls the volume of water flowing on partially wet elements at the flow field boundary (King and Roig, 1988) and contributes to form drag at the element scale (Defina *et al*., 1994). Standard hydraulic modelling assigns a height to each computational node based on interpolation of nearby measurements, and uses a calibrated 'effective' friction coefficient to subsume all other sub-grid scale effects. Hence, such methods can make no use of the sub-grid information available from high-resolution topography data and may suffer from mass and momentum discrepancies because of a failure to account for the correct flow volume. Fortunately, a number of methods have recently been developed that use distribution functions to represent sub-grid scale effects and which can potentially be extended to incorporate otherwise redundant sub-grid scale topographic data into a hydraulic model. Most of these methods concentrate on the problems caused by the inclusion of partially wet elements in the numerical solution during dynamic flooding (King and Roig, 1988; Defina *et al*., 1994; Bates and Hervouet, 1999; Bates, 2000; Defina, 2000). Defina (2000) has also presented a method to parameterize the form drag component of resistance based also on the micro-scale topography within a computational element; however, in this paper we only pursue the former class of sub-grid closure.

The basis of sub-grid corrections for wetting and drying is to introduce a proportionality constant η to scale the shallow water continuity equation on partially wet elements to represent more correctly the true elemental flow volume. For an element with height range $Z_{f\min} \rightarrow Z_{f\max}$, this coefficient takes a value of zero when the element is fully dry (water surface elevation $Z_{felev} = Z_{f\min}$) and a value of one when it is fully wet ($Z_{felev} = Z_{f\max}$). The shape of the η versus Z_f curve for a particular element in the range $Z_{f\min} \rightarrow Z_{f\max}$ is then a function of its sub-grid topography. The distribution functions chosen to represent these curves have ranged from simple linear relationships (e.g. Bates *et al*., 1992; Bates, 2000) to assumptions regarding the self-affine fractal nature of topography (e.g. Defina *et al*., 1994); however, few studies have used topographic data to parameterize directly the shape of the η versus Z_f curves as suggested by Grayson and Blöschl (2001). The exception here is Bates and Hervouet (1999), who obtained LiDAR data consisting of ~800 000 topographic points for a 1×1 km^2 section of tidal mud flat on the eastern coast of the UK. This was used to construct η versus Z_f curves for each element in a ~20 m resolution two-dimensional finite element model of the area. A hypothetical tide was then simulated with this model and the results compared with a control simulation conducted without the sub-grid correction for dynamic wetting and drying. The two simulations showed significant differences in hydrodynamic behaviour during a flood cycle. However, mesh construction was again conducted prior to topography assimilation and no explicit separation of the topography data relevant to grid and sub-grid scales was made. Hence, whilst it was concluded that the wetting and drying algorithm resulted in significant changes in the simulation when compared with the control, the data assimilation method may mean that this conclusion is somewhat flawed.

The purpose of this paper is to provide an example of the optimal assimilation of a spatially dense data set into a complex numerical model that seeks to address the issues identified above. In particular, we are concerned with situations where the data resolution far exceeds that of the computational discretization and use the example of topographic data provision for flood inundation modelling. First, we conduct variogram analysis of LiDAR-derived floodplain topography for the River Stour data set previously analysed by Marks

and Bates (2000) to determine significant horizontal length scales. Second, we describe a method to determine topographically significant points in this data set and explicitly incorporate these into the mesh discretization for two-dimensional hydraulic models using the automatic mesh generator of Horritt (2000). Third, for this discretization we use the data left over from the mesh generation process to parameterize the Bates and Hervouet (1999) sub-grid-scale algorithm for dynamic wetting and drying implemented within a typical two-dimensional finite element solution of the shallow water equations. This model is then compared with the control simulations of flood inundation extent conducted for this reach by Marks and Bates (2000) using a mesh derived independently of topography and with no sub-grid correction algorithm. Ultimately, comparison of various methods of assimilating topography into flood inundation models should be tested against actual hydraulic observations. Bulk flow observations (stage, discharge) from gauging stations cannot perform this task adequately, as differences in topography may be subsumed within the calibration, and one requires some fully distributed data source for a rigorous validation. Inundation extent is an obvious solution here, and it is currently the only distributed hydraulic observation that it is possible to obtain over river floodplains. Though methods have been developed to extract inundation from available satellite synthetic aperture radar (SAR) data (Horritt, 1999; Horritt *et al.*, 2001), these are currently limited to an accuracy of 85–90% of the true inundated area due to the resolution of the imagery (~12·5 m for ERS SAR and RADARSAT) and misclassification errors. The latter result from a lack of fundamental understanding of the interaction of the radar signal with wet soil, emergent and submerged vegetation, the single frequency and polarization modes and the fixed or limited range of incidence angles available on current satellite systems. Though such data and sampling errors are not large, they at present render it impossible to discriminate between competing models (Bates and De Roo, 2000; Horritt and Bates, 2001). Thus, rigorous validation of topographic assimilation methods must await the deployment of new satellite (e.g. ENVISAT, RADARSAT-2, ALOS and TerraSAR) and airborne SAR systems, which potentially provide the required polarimetric or high-resolution capabilities. For this reason, we have not attempted direct validation of the algorithms described in this paper against available inundation extent data, as such a process is likely to prove inconclusive at present. Rather, the purpose of this paper is to develop a methodology for the optimal use of high-resolution data sets in numerical models and test its impact on hydraulic predictions in a given numerical code.

VARIOGRAM ANALYSIS OF LIDAR-DERIVED FLOODPLAIN TOPOGRAPHY

Geostatistical analysis can be used to uncover the spatial structure in distributed data sets (Issaks and Srivastava, 1989), and in this study we wish to determine the spatial autocorrelation in proximal data. Burrough and McDonnell (1998) state that the spatial variation of any variable can be expressed as the sum of three components:

- a structural component, having a constant or mean trend;
- a random, but spatially correlated component,
- a spatially uncorrelated random noise or residual term.

We can represent this spatial dependence using a variogram, in which we plot semivariance, γ (half the expected squared difference between any pair of data) against the lag h (the vector distance and direction of separation between any pair of data) at a particular lag distance:

$$\gamma(h) = \frac{1}{2n} \sum_{i=1}^{n} [z(x_i) - z(x_i + h)]^2 \tag{1}$$

where n is the number of pairs of sample points of attribute z separated by distance h, (Burrough and McDonnell, 1998). A plot of $\gamma(h)$ against h forms the experimental variogram to which a model variogram may then

be fitted in order to describe the spatial patterns in the data. A sample plot showing key parts of a variogram with a model fitted to the data is shown in Figure 1. At large lag values the fitted curve is seen to level off, forming the *sill*; at these lags there is no longer any spatial dependence between pairs of points. The distance between where the curve starts at a low value of $\gamma(h)$ and rises to the sill, is the *range* c_1. This area describes the spatial dependence between related points and defines the maximum lag distance at which spatial dependence still occurs. Finally, the point at which the curve bisects the y—axis marks the *nugget* c_0. This point shows the semivariance present at a lag of zero, namely the semivariance between a point and itself. Thus, the nugget value represents a combination of short-range variation that has not been measured (as it exists at shorter distances than the smallest sampling interval) and random measurement errors (Blöschl and Grayson, 2001). Hence, the nugget allows one to estimate the error present in the data.

The LiDAR data scan pattern approximates to an irregular gridded structure; thus, variogram analysis was performed using the public domain software package GSLIB and its 'Gamv' subroutine, which is designed for irregularly spaced data (Deutsch and Journel, 1998). To minimize computational demands, this routine was applied to four test areas on the River Stour floodplain instead of the complete data set. The full data set and the processing (geoid conversion, vegetation removal, checking for potential systematic errors between flightlines, etc.) applied to it are described in detail in Marks and Bates (2000), and hence the reader is referred to that paper for more information. The test areas were selected to be representative of the whole floodplain and sited away from vegetation (hedges, woodland) or major topographic features, such as embankments, that may have a corrupting influence on the variogram results. The test areas were also sites where measurements were obtained by one flightline only; thus, any possible systematic error present between adjacent flightlines could be discounted at this stage. The characteristics of the four sites are summarized in Table I. For the set of topographic points within each area, the structural component was first removed by fitting a polynomial trend surface to the data. The residual values between the original LiDAR elevations and the corresponding

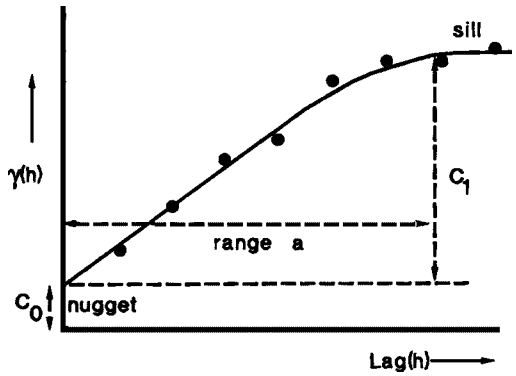

Figure 1. A sample model variogram showing range, nugget, sill (© Peter A. Burrough and Rachael A. McDonnell, 1998. Reprinted from Principles of Geographical Information Systems by Peter A. Burrough and Rachael A. McDonnell (1998) by permission of Oxford University Press

Table I. Summary of test areas used in the variogram analysis

Test area	No. of data points	Size (m^2)	Elevation (m)			SD
			Min	Max	Mean	
1	739	100 × 100	37·645	37·965	37·798	0·055
2	731	100 × 100	36·435	37·485	36·818	0·115
3	751	100 × 100	35·825	36·645	36·139	0·092
4	1313	130 × 130	36·055	40·105	36·422	0·288

horizontal location on the trend surface were then used in the calculation of the variogram. This was achieved by calculating an omnidirectional variogram where all possible directions were combined in a single analysis. Here, we assume that the directional tolerance is large enough to make the direction of any given lag separation vector insignificant and only the magnitude of the lag is important. In effect, we calculate an average of all the possible directional variograms. To avoid problems with clusters of collocated (and hence identical) points obtained at high scan angles with the LiDAR instrument, we used a minimum lag spacing of 3 m (the average spacing between LiDAR points located away from the ends of scan lines) and a tolerance of 1·5 m. The experimental variograms resulting from this analysis are shown in Figures 2 to 5.

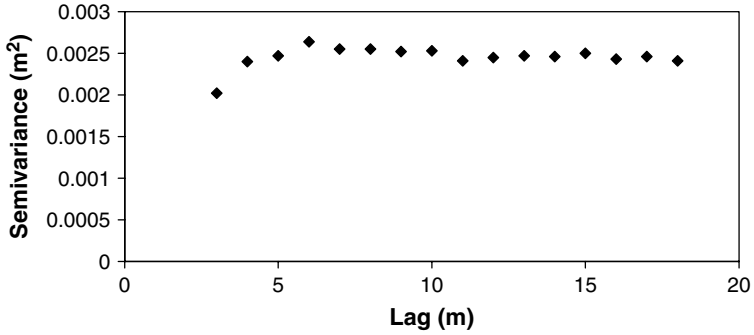

Figure 2. Omnidirectional variogram of test area 1

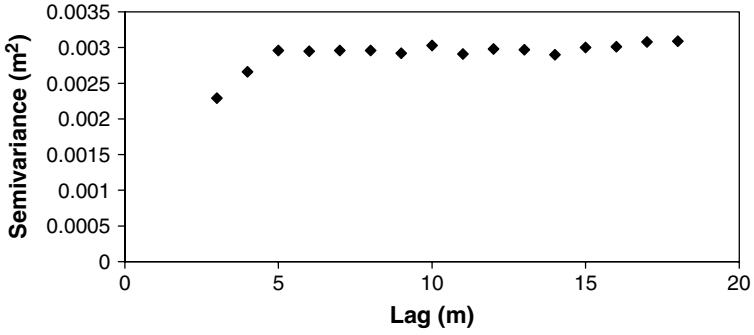

Figure 3. Omnidirectional variogram of test area 2

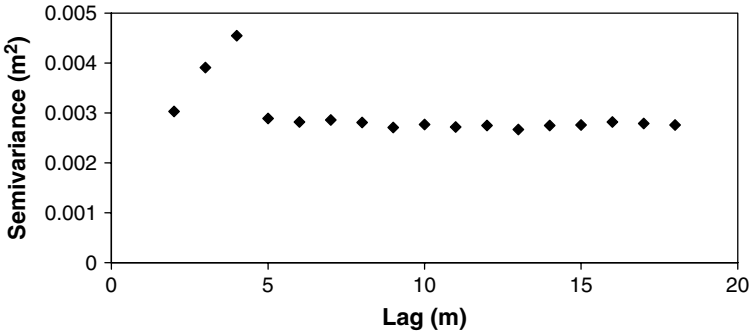

Figure 4. Omnidirectional variogram of test area 3

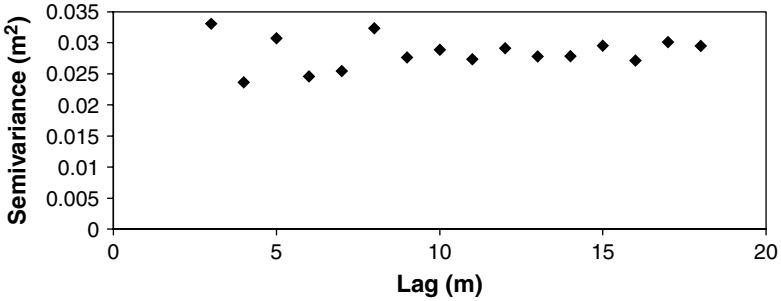

Figure 5. Omnidirectional variogram of test area 4

The omnidirectional variograms for each test area show a high degree of similarity and are largely stable structures that reach a sill at a lag of approximately 7–10 m. Fitting a linear semivariogram model to the data shows a nugget semivariance of 0·008–0·013 m^2. This is broadly equivalent to the quoted 0·15 m RMS error of the LiDAR data (Environment Agency, 1997). Test area 4 reaches a sill at similar lag to areas 1, 2 and 3 and with a low semivariance; however, the structure is very erratic at lower lag spacings. This is because area 4 may contain some data points that represent the top of the vegetation canopy rather than the ground surface and which occur because the vegetation removal algorithm applied to the raw data can never be 100% successful (Marks and Bates, 2000).

Individual variograms of the test areas were also produced along two directional axes to measure the semivariance of the scanline and flightline. This was to see if there was any variation in the spatial dependence scales obtained from the omnidirectional variogram that had been 'masked' in such a generalized measure. For the first variogram, the direction was set along the scanline (60° azimuth). This was constrained to the individual scanlines by using a 1 m tolerance for the bandwidth and a low angular tolerance of ±10°. A flightline transect was also taken by selecting a line at an angle of 320° approximately corresponding to a succession of points measured by different scans along the flightpath of the aircraft. A wide tolerance of ±40 °W was chosen, but again with a constrained bandwidth of 1 m so that elevation measurement points slightly out of line with one another would still be analysed as if they were directly adjacent. The resulting variograms were similar in appearance to the omnidirectional variograms and confirm the scales of spatial dependence shown in Figures 2 to 5.

The above analysis indicates that, below a grid spacing of approximately 10 m, significant spatial dependence between topographic points exists. The variogram range thus provides a general criterion for grid size selection for a given application. This rule relates to the background variability of the topography, and does not account for the length scales of specific features (levees, ditches, often man made) that may have a significant impact on flood hydraulics. However, for finite difference models this analysis may be sufficient to enable a grid size to be selected. For numerical methods, such as the finite element technique, which allow resolution to vary across the domain, we need to go further and identify topographically significant points in order to take full advantage of the method. In this case, the variogram analysis provides a useful insight into what the spacing of these points might be and hence can inform decisions on how many important points may be sufficient to represent the surface. This is explored in the following section.

IDENTIFICATION OF TOPOGRAPHICALLY SIGNIFICANT POINTS FOR AUTOMATED MESHING

Having determined a theoretically appropriate grid spacing based on the typical variogram range in the River Stour data set, we can now proceed to determination of the topographically significant points within the digital elevation model (DEM). A number of methods to accomplish this task have already been developed

for the purpose of converting regular gridded DEM data to a triangular irregular network (TIN) structure. The similarity of TINs with the finite element discretizations employed here means that such methods can be readily adopted, although there are differences between TIN and finite element approaches. In particular, the TIN structure is designed to maximize surface representation and takes no account of numerical stability issues. Most finite element models work best where there is a smooth transition between areas of small and large elements, which promotes stability, and where element shapes are near-regular, which minimizes mass balance errors (see Löhner (2001)). TINs do not necessarily preserve these features and, therefore, we may need to augment the number of points used to represent the surface during the mesh generation process to ensure a stable and mass conservative solution of the controlling equations (see Löhner (2001) for a more complete discussion of grid generation). It should also be noted that to use these methods on irregular topography data, such as that generated by a LiDAR instrument, requires that the data first be converted into a regular grid.

Methods for determining topographically significant points are reviewed by Lee (1991), who saw the purpose of such methods as being to extract the smallest set of points that gives maximum information about the topographic surface. According to Lee (1991), all such methods have two keys steps. These are (1) a method to establish the 'importance' of an elevation point, and (2) specification of a stopping rule that indicates when to terminate the selection process. Points are said to be important when they cannot be easily interpolated using the elevations of neighbouring points; however, a number of methods are available to do this. Thus, Lee (1991) compared three algorithms that extract the subset of significant points from a raster DEM: the very important point (VIP) method (Chen and Guevara, 1987), the hierarchy transform (HT) method (De Floriani *et al*., 1984) and the drop heuristic (DH) method (Lee, 1989). All showed strengths and weaknesses, and these conditioned the circumstances under which each method was appropriate. The VIP method was best suited to the detection of sharp changes in height over short distances and local pits and peaks, but whilst it was computationally efficient it performed less well on gentle slopes. The HT method had a very efficient data structure; however, it tended to produce long thin triangles and distortion was evident in the transition from rugged to flat regions. The DH method provided the closest match to the original DEM, but was computationally demanding as it drops only one point at each iteration and then evaluates all points remaining in the solution set. It is thus only suitable for application to small DEMs. More recent work in this area has concentrated on developing extensions to the HT method (e.g. De Floriani and Puppo, 1995; De Floriani *et al*., 1996; Puppo *et al*., 1997; Brodlie and Wood, 2000) that give multi-resolution representations of a surface for efficient visualization, rather than algorithms to ensure absolute accuracy. Although multi-resolution methods could be used to maximize surface representation, the work by Lee (1991) provides one of the few comparative studies in this area and has hence been used to select the method adopted here.

None of the above methods is ideal for LiDAR data of river floodplains, as such data sets are typically extremely large (of the order of a gigabyte) and contain both areas of very flat relief and sharp breaks of slope to linear features and structures (embankments, levees, terraces, etc.). The latter are hydraulically very significant to inundation development and need to be accurately represented in any flow model. Further, we should select a method that best respects the requirements of finite element models. These constraints rule out both the HT and DH methods in favour of the VIP method, despite its relative underperformance in areas of low slope. The VIP method passes a 3×3 window (whose width should clearly be no greater than the variogram range) over all the points of a grid and for each sees how well the eight surrounding grid points interpolate it along the cardinal and inter-cardinal profile lines. This is done simply by the sum of errors between the observed and interpolated heights. Points deemed well estimated are also deemed unimportant, as they can be replicated accurately by their neighbouring points; therefore, points are selected based on their significance in describing the surface. After the initial pass of the filter, the most significant points within the mesh are selected first, with less-significant points being added to the output point coverage until a user-specified cut off is reached. This stopping rule is defined in terms of a maximum number of significant points in the output coverage and is based on a compromise between

the computational resources available and the global rule for nodal spacing determined from the variogram analysis. This point coverage can then be subsequently converted into a TIN or, as in our case, a model discretization.

To use this method on the 261 634 irregular points in the raw LiDAR data set requires that these first be gridded. However, if a cell contains no data the algorithm automatically assigns it a high significance. As the maximum horizontal spacing of the 'raw' LiDAR data was ~4 m, a 5 m grid was used to ensure that no blank cells remained in the gridded coverage. Coincidentally, this spacing also means that the width of the 3×3 VIP filter is 10 m and identical to the range identified in the variogram analysis. This also had the advantage of 'thinning' the data, so as to prevent the generation of excessively thin (and thus potentially unstable) elements within the output mesh. In this way the total number of points in the final 5 m gridded DEM decreased to 96 213. The reason for this large reduction is that certain areas of the floodplain have point densities in the 'raw' data set of much greater than one per ~4 m. In particular, points cluster together at the ends of scan lines, and higher point densities are obtained in areas where the swaths from two different flightlines overlap.

Once gridded, the VIP procedure was run on the data using the stopping rule that the final output should contain ~2% of the points in the input coverage. This was chosen, as here the mesh generation process was subject to the additional constraint that we wished the final topographically optimum mesh to have approximately the same number of nodal points as the topographically independent mesh of Marks and Bates (2000). This was both to facilitate a rigorous comparison and to control against the possibility that the model calibration might not be stationary with respect to scale. The model constructed by Marks and Bates (2000) had 6049 nodes and 11 265 triangular elements with an average size of ~30 m per side. This represented the most dense discretization that was computationally feasible when the original simulations were conducted in 1998, but its resolution is clearly coarser than the ~10 m global spacing rule indicated by variogram analysis. In this case, the trade off between the ~10 m global spacing rule and ~30 m resolution based on 1998 computational constraints was skewed towards the latter. The 2% threshold was found to produce 2173 points classified as being topographically important within the domain. When combined with nodes representing the channel (2885), the domain boundary (831) and the lower end of the domain beyond the LiDAR coverage (573), this gave a total 6462 significant points to be used in mesh generation.

As noted above, of the methods reviewed by Lee (1991) the VIP method best respects good discretization principles for finite element methods. However, it does not explicitly follow such guidelines and, therefore, needs to be used in conjunction with a mesh generator that can both be forced to honour specific points and add additional points to create a smoothly varying mesh of regular element shapes. For two-dimensional triangular elements, mesh generators are typically based on a conforming Delaunay triangulation that meets constraints on minimum internal angle and maximum area for each element. Whilst a substantial literature concerned with the generation of such meshes exists (e.g. Frey, 1987; Frey and Field, 1991; Rebay, 1994), and techniques for adapting meshes to the spatial properties of finite element solutions are available (Knupp, 1995), specific mesh generators for fluvial applications are rare. One of the few available is the Cheesymesh programme of Horritt (2000), a derivative of the Easymesh code developed by Bojan Niceno at the Technical University of Delft, The Netherlands. This meets the above criteria for mesh quality, and also enables the incorporation of a regularly meshed channel within an irregularly meshed domain. This is required for fluvial applications as, in order to reduce computational constraints, it is usual to elongate channel elements in the downstream direction (e.g. Gee *et al*., 1990; Feldhaus *et al*., 1992; Bates *et al*., 1998). Cheesymesh determines the elongation ratio for these elements using a criterion based on local channel curvature (see Horritt (2000)). This was determined through comparison of numerical and analytical solutions of the shallow water equations for a range of computational grids. Cheesymesh is therefore an ideal mesh generator for this class of application and has a robust physical basis.

The discretization derived from Cheesymesh using the points determined by the VIP method is shown in Figure 6b and compared with the original topographically independent mesh of Marks and Bates (2000)

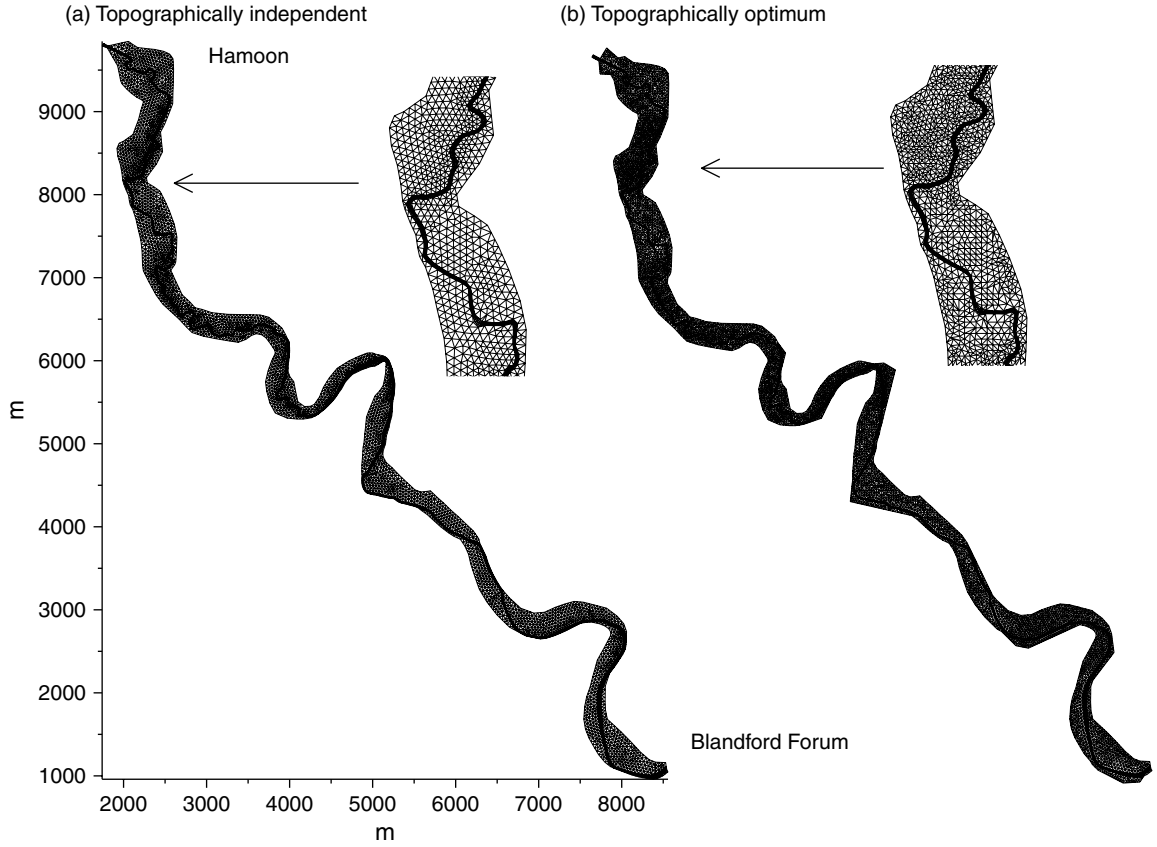

Figure 6. Finite element meshes developed for a 12 km reach of the River Stour, Dorset, UK, using (a) topographically independent and (b) topographically optimum discretization methodologies

in Figure 6a. The final number of computational points in the new discretization is 8132, connected as 15 396 elements with an average length per side of ~25 m. Cheesymesh has therefore needed to add 1670 points to the coverage in order to obtain a conforming finite element mesh capable of preserving solution quality. At these points the topographic value is assigned by weighted nearest-neighbour interpolation. The same channel topography is used for both models, and is based on 25 cross-sections surveyed by the UK Environment Agency. The topography as incorporated into each model is shown in Figure 7, and cross-sections through each discretized topographic surface are shown in Figure 8 and compared with the raw topography data. Figure 8 shows differences between the two surfaces that are likely to be hydraulically significant. Differences of several metres are indicated in certain places, and, in general, the mesh generated using the VIP algorithm follows the original surface better, particularly for cross-sections B, C and D. For cross-section A, both topographically independent and topographically optimum meshes are similarly in error compared with the original data. These differences result from the coarse model grid (~30 m), compared with the LiDAR data, and the need to undertake interpolation to compare unstructured grids with different topologies. This means that each model floodplain cross-section is defined by interpolation from only six to eight nodes on each bank, which can be up to ~15 m from the interpolated section and can lie on surfaces with substantially different elevations (levees, embankments, bank collapses, etc.). Misrepresentation of any of these is likely due to the coarse spatial sampling of the finite element grids if important points are not identified and this will lead to the observed errors in interpolated cross-sections. Overall, though the

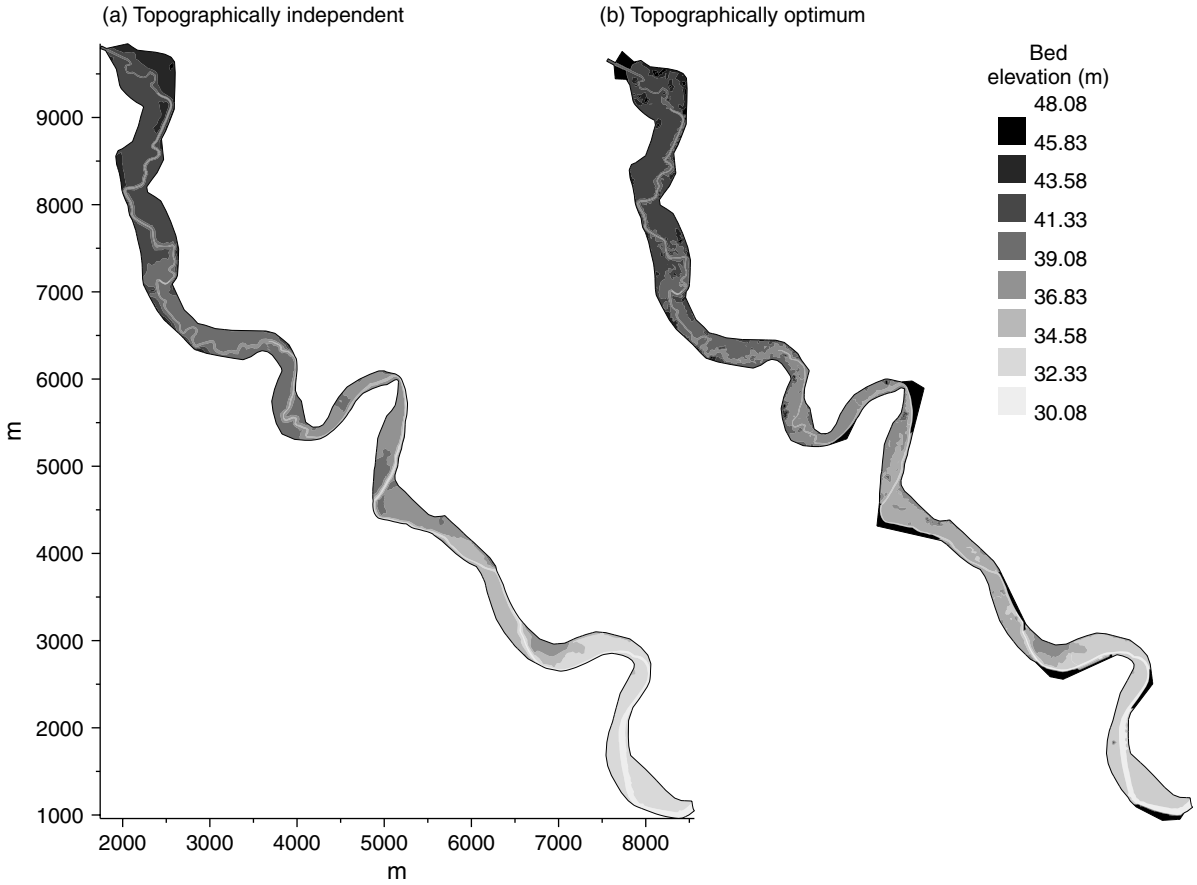

Figure 7. Topographic surface represented by the (a) topographically independent and (b) topographically optimum discretization methodologies shown in Figure 6

method developed in this paper is still not an ideal representation of the original surface, it is a substantial improvement over earlier mesh generation methods. One can also note the lateral shift in channel location of up to 10 m between the map data (surveyed in 1961) from which the channel location was digitized and the LiDAR survey (taken in 1997). Although we cannot be certain of the accuracy of this figure, some channel movement is to be expected in a dynamic river environment, and this will introduce additional error.

USE OF REDUNDANT DATA FOR PARAMETERIZATION OF SUB-GRID SCALE CORRECTIONS FOR DYNAMIC WETTING AND DRYING

For each element in the topographically optimum mesh the sub-grid topography was used to parameterize directly the wetting and drying algorithm of Bates and Hervouet (1999). This algorithm is described fully in a number of previous papers (Bates and Hervouet, 1999; Bates, 2000) and, therefore, is only briefly reviewed here. The algorithm is designed for use with the two-dimensional shallow water equations, which can be expressed in non-conservative form as:

Mass conservation

$$\frac{\partial h}{\partial t} + \boldsymbol{u}\cdot\mathrm{grad}(h) + h\mathrm{div}(\boldsymbol{u}) = 0 \tag{2}$$

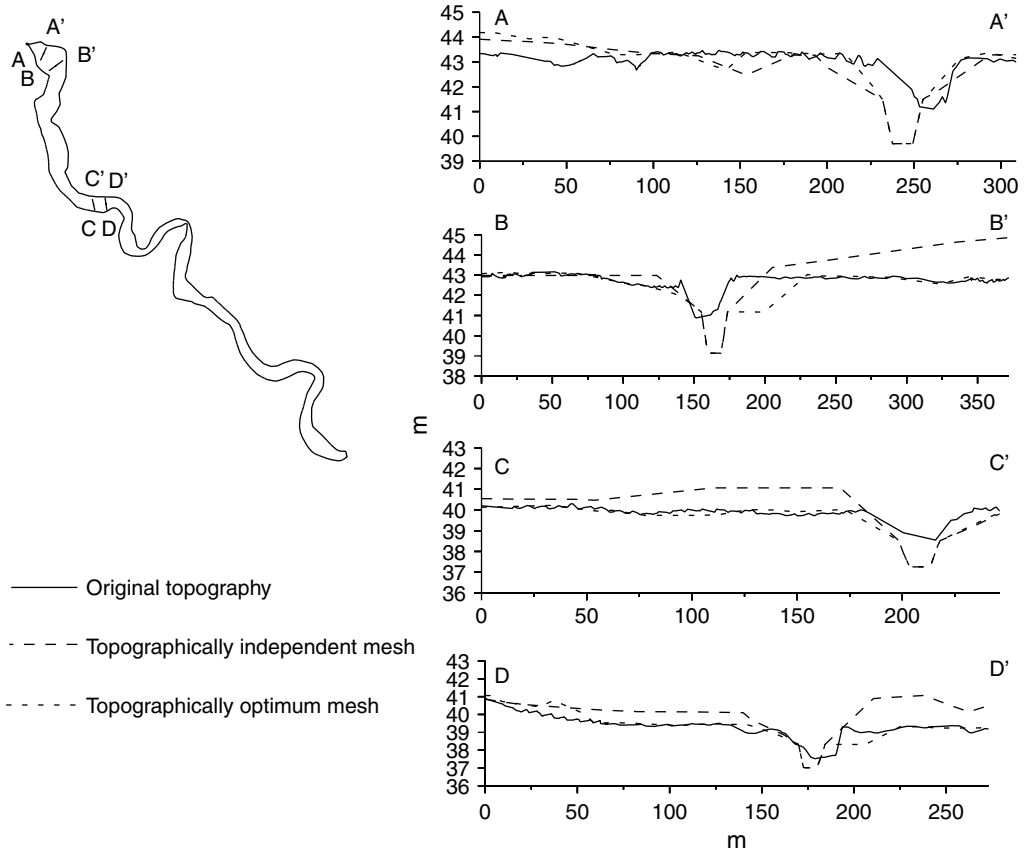

Figure 8. Comparison of four cross-sections taken through the two topographic surfaces shown in Figure 7

Momentum conservation

$$\frac{\partial u}{\partial t} + \boldsymbol{u}\cdot\mathrm{grad}(u) + g\frac{\partial h}{\partial x} - \frac{1}{h}\mathrm{div}(\nu_t h\ \mathrm{grad}(u)) = S_x - g\frac{\partial Z_f}{\partial x} \tag{3}$$

$$\frac{\partial v}{\partial t} + \boldsymbol{u}\cdot\mathrm{grad}(v) + g\frac{\partial h}{\partial y} - \frac{1}{h}\mathrm{div}(\nu_t h\ \mathrm{grad}(v)) = S_y - g\frac{\partial Z_f}{\partial y} \tag{4}$$

where u and v are the depth-averaged velocity components [with dimensions LT^{-1}] in the x and y Cartesian directions [L], h is the depth of flow [L], Z_f is the bed elevation [L], ν_t is the turbulent viscosity [L^2T^{-1}], S_x and S_y are the source terms (friction, Coriolis force and wind stress), g is the gravitational acceleration [LT^{-2}], and t is the time [T].

For moving boundary problems, such as dynamic flooding, solved on fixed numerical grids, a number of problems arise with the numerical solution of Equations (2) to (4) as a result of the partially wet elements that occur at the flow field boundary (see Lynch and Gray (1980) for a discussion). This is a consequence of attempting to simulate a continuous water surface with a discrete numerical grid and generates incorrect predictions of mass and momentum flux in such zones. Numerical instability may also be manifest, as small changes in water depth can bring large numbers of elements into and out of the solution, thereby generating spurious oscillations in boundary position. Bates and Hervouet (1999) also show that poor representation of shallow water hydraulics can have adverse impacts over the whole flow domain.

The basis of wetting and drying algorithms for fixed grid models is to try to represent better the shallow water hydraulics on partially dry elements (e.g. King and Roig, 1988; Defina *et al*., 1994; Bates and Hervouet, 1999; Defina, 2000). The Bates and Hervouet (1999) algorithm is typical of this class of solution and was chosen here as it is relatively simple and is the only algorithm that incorporates both mass and momentum corrections. Momentum is corrected using the methodology of Hervouet and Janin (1994). Here, partially wet elements are included within the domain and the dominant driving term in the momentum equation is assumed to be:

$$\frac{\partial u}{\partial t} = -g\frac{\partial h}{\partial x} \tag{5}$$

Other terms, e.g. friction and diffusion, still act on such an element but are relatively unimportant. The above water slope term may then be cancelled or replaced to prevent the development of unrealistic velocities due to the spurious non-zero free surface gradient across the element. Mass conservation is ensured using the sub-grid scaling method developed independently by King and Roig (1988) and Defina *et al*. (1994). Here, a scaling coefficient η is defined which varies from zero to one for each element as it tends from fully dry (zero) to fully wet (one). This coefficient is then used to scale the continuity equation to represent the true volume of water residing on that element at each time step. According to Defina *et al*. (1994), the continuity Equation (2) thus becomes:

$$\eta\frac{\partial h}{\partial t} + \vec{\boldsymbol{u}}\cdot\mathrm{grad}(h) + h\mathrm{div}(\vec{\boldsymbol{u}}) = 0 \tag{6}$$

η, therefore, varies with water depth, and the form of the relationship between η and h is dependent on the sub-grid topography (i.e. $\eta = f(Z_\mathrm{f}, h)$).

The η versus Z_f curves were then calculated for the River Stour LiDAR data using the method outlined by Bates and Hervouet (1999) and Bates (2000). For each element in the mesh a Delaunay triangulation of the sub-grid topographic points plus the three element vertices was generated. This led to a highly detailed representation of sub-grid topographic variations. In effect, we have replaced a large planar element with a set of smaller sub-grid planar triangles from which we can more accurately calculate the proportion of the element inundated for a given free surface elevation. The functions $\eta = f(Z_\mathrm{f})$ with η varying from zero to one were discretized in terms of 20 piecewise linear segments representing 5% increments of inundation extent. This proved sufficient to represent the $\eta = f(Z_\mathrm{f})$ curves as a smoothly varying function. It should be noted that, for a topographically independent mesh, the range of sub-grid topography can potentially be wider than the height range over an element and hence η does not vary between zero and one over the element height range. This can generate discontinuities as elements enter or are removed from the numerical solution. Use of the VIP algorithm should alleviate this problem: elements should not contain local maxima and minima, as these will be automatically selected as computational nodes.

To assign η values at time step t for a given element we take, at time t^{-1}, the water free surface elevation of the node with maximum depth as being the 'true' regional water free surface elevation. η is then linearly interpolated from the $\eta = f(Z_\mathrm{f})$ curve for that element and used explicitly to evaluate Equation (6) at time t.

MODEL TESTING AND ANALYSIS

For each discretization shown in Figure 6 a 1 in 4 year flood event was simulated that took place over 62 h on and around 20 December 1993. Flows were monitored at nationally maintained gauging stations located at the up- and down-stream ends of the reach and provided the boundary conditions for the model. These consisted of an imposed discharge at the upstream boundary and an imposed stage at the downstream boundary. This gives a well posed numerical problem, provided there is no recirculation at the downstream end. The event was discretized into 55 800 time steps of 4 s duration, with initial conditions based on steady-state flow calculated using the gauged discharge and stage at the start of the event. For the dynamic simulations, boundary conditions consisted of upstream discharge and downstream stage hydrographs. Identical friction factors were assigned

to each model based on the calibration of the topographically independent mesh conducted by Marks and Bates (2000), which disaggregated the model domain into two areas: channel and floodplain. Calibration was achieved by manipulating the floodplain friction factor (to which the model was most sensitive) to replicate the timing of peak discharge at the downstream boundary only. All other aspects of the hydrograph (shape, volume, peak magnitude, etc.) were left to vary freely. Final values for the friction specified in terms of Manning's n were 0·017 for the channel and 0·035 for the floodplain.

Simulations were conducted using the modified version of the TELEMAC-2D model developed by Bates and Hervouet (1999), which solves Equations (3), (4) and (6) for a finite element mesh of linear triangular elements with computational nodes located at the element vertices. Hence, water depth and the two components of the depth-averaged velocity vector are calculated and both sub- and super-critical flow regimes can be handled. A fractional step method (Marchuk, 1975) is used, where advection terms are solved initially, separate from the propagation, diffusion and source terms which are solved together in a second step. For the advection step, several schemes may be used, with the Method of Characteristics chosen here for the momentum equation. To ensure mass conservation, the Streamline Upwind Petrov Galerkin (SUPG) method (Brookes and Hughes, 1982) has been applied for the advection of h in the continuity equation. Though developing a model using the non-conservative shallow water equations may result in greater problems with mass conservation, their use is justified here; this is because in the conservative equations, discharge is the main unknown, and to recover velocities one needs to divide by the water depth. This is a significant problem for calculations that involve dynamic wetting and drying of the domain as the water depth goes to zero. Such problems are reduced by use of the non-conservative form, and hence this was chosen for the simulations reported here. Turbulence was represented using a zero-equation closure scheme, although, given the element sizes employed, the final scheme was rather insensitive to the values of ν_t in a physically realistic range ($\nu_t = U_* h$, where U_* is the shear velocity). The turbulent viscosity was therefore set at the upper end of this range, at 2·0 $m^2\ s^{-1}$, although a lower value could easily have been used. The precision of the numerical solver was set at 1×10^{-4}.

Three simulations were conducted with this model: a control simulation with the topographically independent mesh and two simulations with the topographically optimum mesh developed here, one with the sub-grid correction and one without. Mass balance performance was similar for each model (seeTable II), although the topographically independent model performed better in this respect. This is likely to be because this mesh has not been forced to honour specific topographic points, and thus its elements are rather more regular (see inset in Figure 6). Further work is thus required on techniques to turn a set of irregular data points into a conforming finite element mesh that can better preserve mass balance. Figure 9 shows the downstream predicted discharge for each simulation compared with the observed discharge at the Blandford Forum gauging station. Although stage at this point has been used as a model boundary condition, the calibration strategy adopted was based on replicating timing of peak stage only. Hence the discharge is at least quasi-independent of the model and can provide some information on model performance. Differences between the simulations show that changing topographic representation does have some effect on bulk flow prediction, but these differences are small and, as anticipated, could be subsumed within a calibration process.

Table II. Mass balance performance for each model

Model	Average instantaneous mass balance error ($m^3\ s^{-1}$)	Average mass balance error per time step (% of initial volume within the domain)	Mass lost as a percentage of hydrograph volume (%)
Topographically independent	1·12	$2{\cdot}75 \times 10^{-6}$	1·37
Topographically optimum	4·68	$1{\cdot}03 \times 10^{-5}$	5·75
Topographically optimum plus sub-grid scale correction for dynamic wetting and drying	5·38	$1{\cdot}18 \times 10^{-5}$	6·61

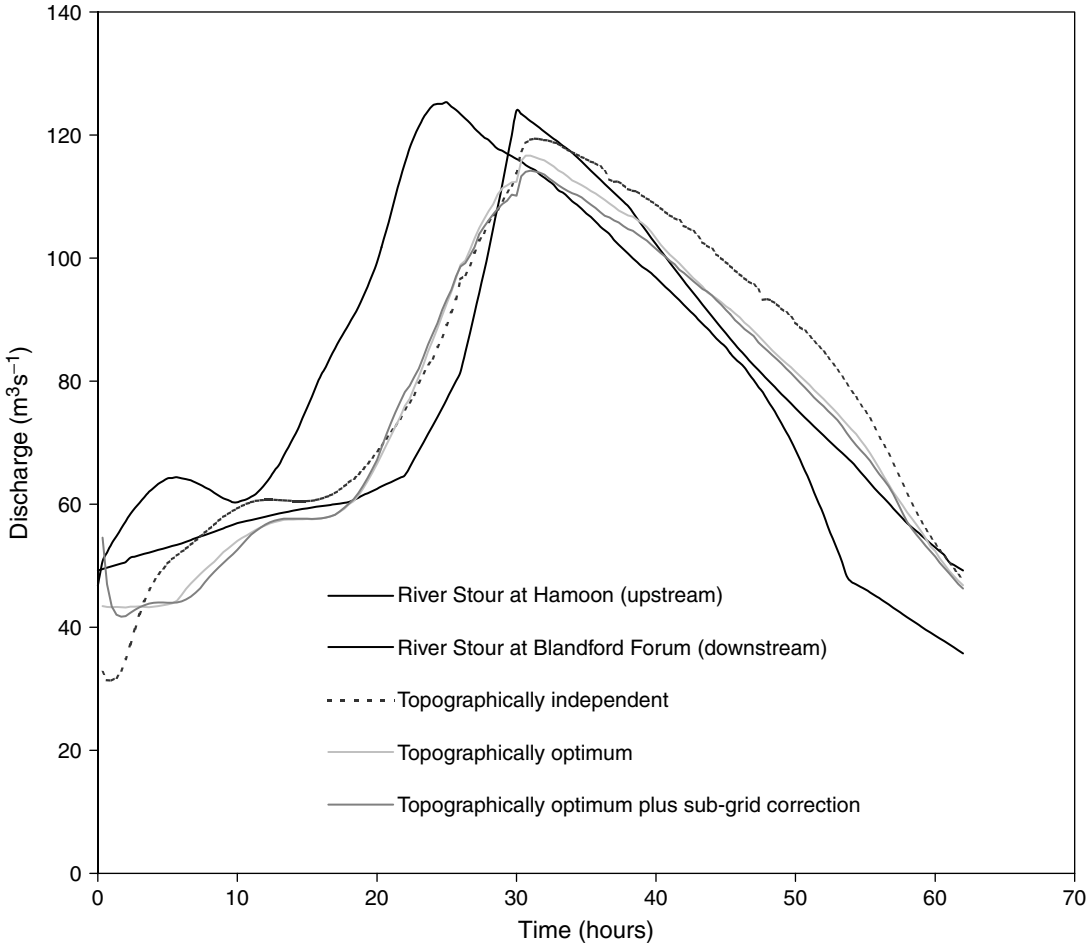

Figure 9. Comparison of observed and predicted downstream hydrographs for the three simulations conducted in this study

Figure 10 shows water depths predicted by each model at three time steps during the simulation: during the rising limb ($t = 13$ h), at peak inundation ($t = 33$ h) and at the end of the simulation when the hydrograph has passed out of the domain ($t = 62$ h). Significant differences in inundation extent between these models are shown on the rising limb and at the end of the event. These are shown in more detail for two areas of the floodplain on the rising limb of the hydrograph in Figure 11. At the end of the event, the differences between simulations are likely to be due to water ponded on the floodplain as a result of better incorporation of topographic minima in the topographically optimum model. These will drain only slowly, if at all, and ultimately we may require some kind of surface infiltration algorithm (e.g. Stewart *et al*., 1998) to simulate de-watering of the floodplain. At peak inundation, differences in inundation extent are much less marked, although differences in water depths do exist. This is confirmed in Figure 12, which shows stage hydrographs through the event at three floodplain locations. This is because at peak flow the inundation boundary lies towards the edge of the floodplain on areas of higher slope, where differences in water depth do not translate into differences in boundary position. This is significant, as most inundation data record either maximum extent (e.g. post-event reconstructions from trash lines, tide marks, etc.) or are collected at or around the

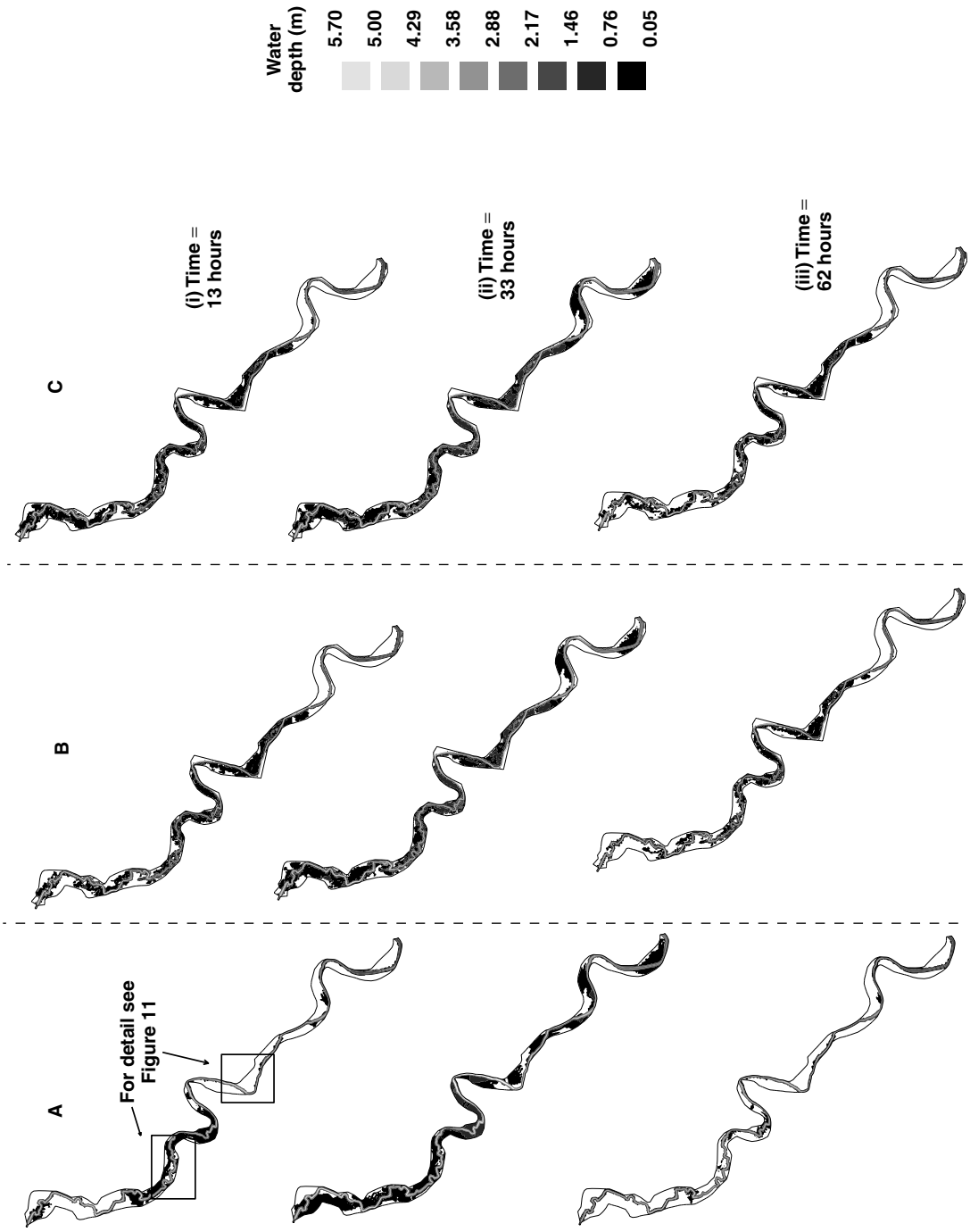

Figure 10. Water depths at three time steps during the 62 h flood simulation for (A) the topographically independent mesh, (B) the topographically optimum mesh, and (C) the topographically optimum mesh simulated with a correction for dynamic wetting and drying. The time steps shown correspond to (i) the hydrograph rising limb at 13 h, (ii) peak inundation at 33 h, and (iii) the end of the simulation at 62 h when the hydrograph has fully passed through the reach

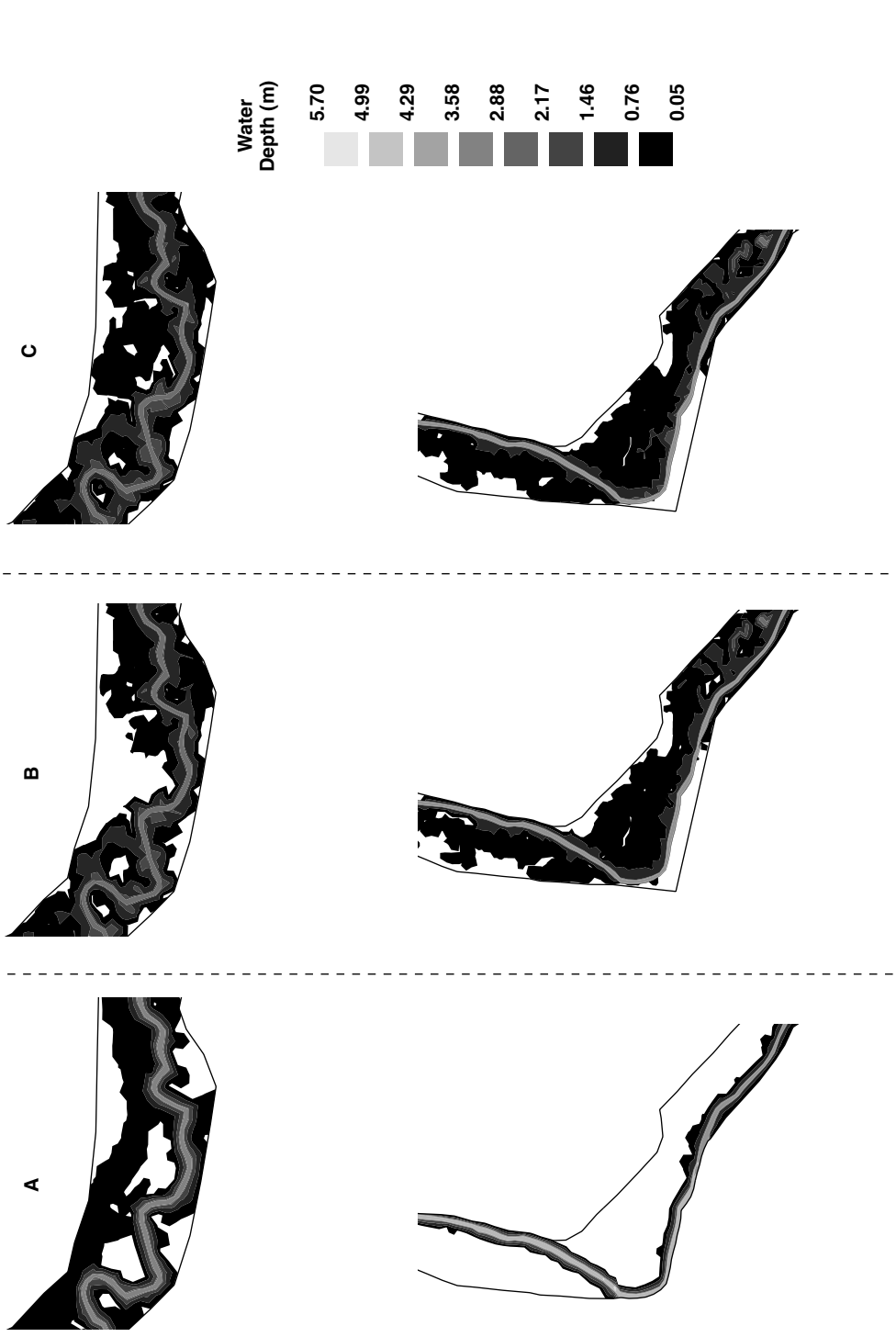

Figure 11. Detailed images of water depths predicted within the two inset boxes shown in Figure 10 at 13 h into the simulation. The images represent (A) the topographically independent mesh, (B) the topographically optimum mesh, and (C) the topographically optimum mesh simulated with a correction for dynamic wetting and drying. Note the significant differences between the topographically independent and topographically optimum models, and to a lesser extent the differences created by inclusion of the sub-grid correction for wetting and drying

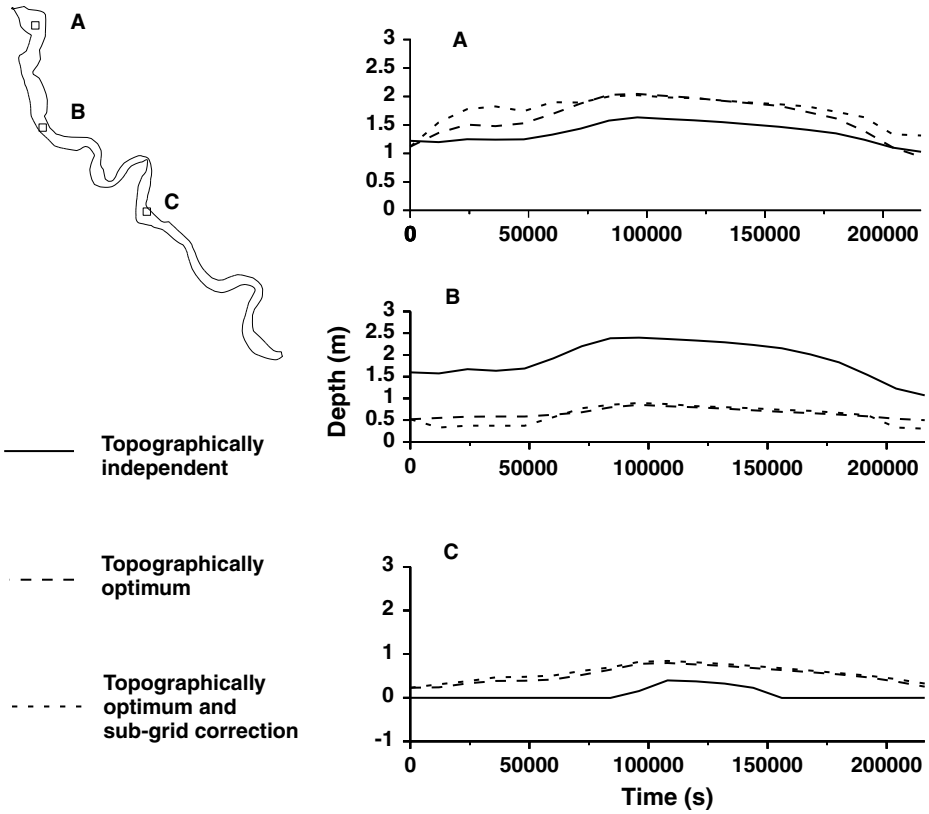

Figure 12. Stage hydrographs at three floodplain locations (A, B and C) for the three simulations conducted in this study

time of peak inundation (e.g. airborne surveys of flood extent for use by civil protection authorities). This is also true of most satellite images of flood extent (e.g. Bates and De Roo, 2000), which tend only to be retrieved from the archive for major floods and at the time of the flood peak. This analysis indicates that none of these data sources is likely to prove optimum for model validation. Rather, we require sampling of a number of synoptic images of flood extent through an event, and particularly on the short-duration rising limb.

The most significant differences in water depth are caused by changing the discretization. Addition of the sub-grid wetting and drying correction has some additional effect in certain areas (e.g. area 1 on Figure 11), but in general these are much less pronounced. Nevertheless, this study indicates that both determination of topographically significant points and sub-grid correction for dynamic wetting and drying should be adopted for two-dimensional modelling of inundation extent when high-resolution topography data are available.

CONCLUSIONS AND FUTURE RESEARCH NEEDS

This paper has described a processing chain for the optimum incorporation of high-resolution topographic data into flood inundation models. This consists of: (i) an assessment of significant length scales of variation in the input data sets; (ii) determination of significant points within the data set; (iii) translation of these into a conforming model discretization that preserves solution quality for a given numerical solver; and (iv) incorporation of otherwise redundant sub-grid data in a computationally efficient manner. Whilst any given element of this chain can be replaced as more effective methods are developed, its basic structure

would appear reasonable and leads to significant differences in hydraulic predictions when compared with a control simulation. For example, height differences between the topographically optimum and topographically independent meshes were up to 2 m, and this led to corresponding differences in water depth. This basic approach is likely to be useful for any data set where the resolution exceeds that of the model in which it is to be used.

An important area for further study is to replicate the analysis conducted here for other floodplains and other high-resolution topography data sets to determine how general the conclusions regarding significant length scales are. This should indicate whether there are thresholds between 'information' and 'noise' that are transferable between different floodplains or classes of floodplains. A second area for research should be directed at enhancing certain components of the processing chain. Thus far we have used available algorithms; however, even this preliminary analysis has demonstrated a number of areas where, for flood inundation modelling, we require development of specific processing techniques. In particular, we require an algorithm capable of determining significant points in irregular data, rather than being forced to first grid the data as with the methods explored here. This may mean that we need more rigorous ways of identifying significant points and may ultimately place more stress on the mesh generation phase if the 'irregular VIP' algorithm generates a highly distorted discretization.

It is also clear that we need methods to identify and connect linear topographic features in the LiDAR data, given their significant hydraulic impact. None of the methods described in this paper does this explicitly, and their ability in this respect needs to be explored further. Similarly, the variogram analysis suggests that we need to improve vegetation removal algorithms used on LiDAR data to distinguish better between vegetation and ground hits. We should also recognize that the simulations developed in this paper still make use of a spatially lumped and calibrated friction surface. This is the other key unknown in flood inundation modelling and can also potentially be determined from LiDAR data. Frictional resistance on floodplains is dominated by drag due to vegetation. Studies have shown that vegetational resistance is determined by an interaction between certain plant biophysical properties (height, stiffness, etc.) and flow (Kouwen and Li, 1980; Fathi-Moghadam and Kouwen 1997; Kouwen and Fathi-Moghadam 2000; Kouwen, 2000) and that these biophysical properties all correlate with plant height (Temple, 1987). Vegetation height can be calculated from LiDAR data as part of its standard processing chain, and hence can be used to assign spatially and temporally variable friction coefficients to a hydraulic model. Preliminary studies two-dimensional finite element codes have already been conducted by Mason *et al*. (submitted), and we now require research to unify this with the techniques for the optimum specification of topography developed here. In the medium term one can envisage a system capable of, at least semi-automatically, generating an optimal discretization that captures both significant topographic features (embankments, levees) and vegetation patches (hedges, stands of trees), coupled with direct parameterization of sub-grid-scale topographic and frictional effects. The need for calibration of such a model should be minimized, and one might thus expect some reduction in predictive uncertainty. In practical terms this would be a major step towards increasing forecast skill for flood inundation codes.

Finally, and perhaps most importantly, we require a rigorous validation data set in order to determine the absolute rather than relative utility of these developments and begin to discriminate between competing approaches. The analysis presented in this paper begins to indicate what the characteristics of such a data set might be. We clearly need high resolution and accurate inundation extent data sampled synoptically a number of times through a flood hydrograph. In particular, we require data from the short-duration rising limb, as this is where we anticipate we will have the best opportunity to discriminate between competing approaches. Data at peak inundation are less helpful, and data on the falling limb are likely also to record static ponding of water on the floodplain, which is rather easier to model, as well as true dynamic effects. Ideally, such data would be supplemented by stage records from a number of locations internal to the model domain, which although only zero-dimensional in space are one-dimensional in time and would allow actual model variables rather than binary pattern information (e.g. Aronica *et al*., 2002) to be validated. Collection of such data would be a major logistical exercise, but is probably the only way to validate currently available inundation codes rigorously.

ACKNOWLEDGEMENTS

The authors wish to thank the UK Environment Agency, and in particular staff at the National Centre for Environmental Data and Surveillance, for provision of LiDAR and flow data used in this analysis. KJM was supported by a studentship made available by the UK Natural Environment Research Council (NERC). Additional support was also obtained from NERC grant GR3 CO/030 and the EU Framework 5 grant 'Development of a European Flood Forecasting System (EFFS)'. The TELEMAC code was made available to University of Bristol by Electicité de France, Laboratorie National d'Hydraulique.

REFERENCES

Aronica G, Bates PD, Horritt MS. 2002. Assessing the uncertainty in distributed model predictions using observed binary pattern information within GLUE. *Hydrological Processes* **16**: 2001–2016.

Bates PD. 2000. Development and testing of a sub-grid scale model for moving boundary hydrodynamic problems in shallow water. *Hydrological Processes* **14**: 2073–2088.

Bates PD, De Roo APJ. 2000. A simple raster-based model for floodplain inundation. *Journal of Hydrology* **236**: 54–77.

Bates PD, Hervouet J-M. 1999. A new method for moving boundary hydrodynamic problems in shallow water. *Proceedings of the Royal Society of London, Series A: Mathematical and Physical Sciences* **455**: 3107–3128.

Bates PD, Anderson MG, Baird L, Walling DE, Simm D. 1992. Modelling floodplain flow with a two dimensional finite element scheme. *Earth Surface Processes and Landforms* **17**: 575–588.

Bates PD, Stewart MD, Siggers GB, Smith CN, Hervouet J-M, Sellin RHJ. 1998. Internal and external validation of a two dimensional finite element model for river flood simulation. *Proceedings of the Institution of Civil Engineers, Water Maritime and Energy* **130**: 127–141.

Blöschl G, Grayson R. 2001. Spatial observations and interpolation. In *Spatial Patterns in Catchment Hydrology: Observation and Modelling*, Grayson R, Blöschl G (eds). Cambridge University Press: Cambridge, UK; 17–50.

Beven KJ. 1989. Changing ideas in hydrology: the case of physically based distributed models. *Journal of Hydrology* **105**: 79–102.

Brodlie K, Wood J. 2000. Recent advances in volume visualisation. *Computer Graphics Forum* **20**: 125–148.

Brookes AN, Hughes TJR. 1982. Streamline upwind/Petrov Galerkin formulations for convection dominated flows with particular emphasis on the incompressible Navier–Stokes equations. *Computer Methods in Applied Mechanics and Engineering* **32**: 199–259.

Burrough PA, McDonnell RA. 1998. *Principles of Geographic Information Systems*. Oxford University Press: Oxford, UK; 333 pp.

Chen Z-T, Guevara JA. 1987. Systematic selection of very important points (VIP) from digital terrain model for constructing triangular irregular networks. In *Proceedings of AUTO-CARTA 8*, Chrisman N (ed.). American Congress of Surveying and Mapping: Falls Church, USA; 50–56.

Cline DW, Bales RC, Dozier J. 1998. Estimating the spatial distribution of snow in mountain basins using remote sensing and energy balance modelling. *Water Resources Research* **34**: 1275–1285.

Defina A. 2000. Two-dimensional shallow flow equations for partially dry areas. *Water Resources Research* **36**: 3251–3264.

Defina A, D'Alpaos L, Matticchio B. 1994. A new set of equations for very shallow water and partially dry areas suitable to 2D numerical models. In *Modelling Flood Propagation Over Initially Dry Areas*, Molinaro P, Natale L (eds). American Society of Civil Engineers: New York; 72–81.

De Floriani L, Puppo E. 1995. Hierarchical triangulation for multi-resolution surface description. *ACM Transactions on Graphics* **14**: 363–411.

De Floriani L, Falcidieno B, Nagy G, Pienovi C. 1984. A hierarchical structure for surface approximation. *Computer and Graphics* **8**: 183–193.

De Floriani L, Marzano P, Puppo E. 1996. Multi-resolution models for topographic surface description. *Visual Computer* **12**: 317–345.

Deutsch CV, Journel AG. 1992. *GSLIB: Geostatistical Software Library and User's Guide*. Oxford University Press: Oxford, UK; 369 pp.

Environment Agency. 1997. *Evaluation of the LiDAR Technique to Produce Elevation Data for use Within the Agency*. UK Environment Agency, National Centre for Environmental Data and Surveillance: Bath, UK; 33 pp.

Fathi-Maghadam M, Kouwen N. 1997. Nonrigid, nonsubmerged, vegetative roughness on floodplains. *Journal of Hydraulic Engineering, American Society of Civil Engineers* **123**: 51–57.

Feldhaus R, Höttges J, Brockhaus T, Rouvé G. 1992. Finite element simulation of flow and pollution transport applied to a part of the River Rhine. In *Hydraulic and Environmental Modelling; Estuarine and River Waters*, Falconer RA, Shiono K, Matthews RGS (eds). Ashgate Publishing: Aldershot; 323–344.

Franks SW, Gineste P, Beven KJ, Merot P. 1998. On constraining the predictions of a distributed model: the incorporation of fuzzy estimates of saturated areas into the calibration process. *Water Resources Research* **34**: 787–797.

Frey WH. 1987. Selective refinement: a new strategy for automatic node placement in graded triangular meshes. *International Journal of Numerical Methods in Engineering* **24**: 2183–2200.

Frey WH, Field DA. 1991. Mesh relaxation: a new technique for improving triangulations. *International Journal of Numerical Methods in Engineering* **31**: 1121–1133.

Gee DM, Anderson MG, Baird L. 1990. Large scale floodplain modelling. *Earth Surface Processes and Landforms* **15**: 512–523.

Grayson R, Blöschl G. 2001. Spatial modelling of catchment dynamics. In *Spatial Patterns in Catchment Hydrology: Observation and Modelling*, Grayson R, Blöschl G (eds). Cambridge University Press: Cambridge, UK; 51–81.

Hervouet J-M, Janin J-M. 1994. Finite element algorithms for modelling flood propagation. In *Modelling Flood Propagation Over Initially Dry Areas*, Molinaro P, Natale L (eds). American Society of Civil Engineers: New York; 102–113.

Horritt MS. 1999. A statistical active contour model for SAR image segmentation. *Image and Vision Computing* **17**: 213–224.
Horritt MS. 2000. Development of physically based meshes for two dimensional models of meandering channel flow. *International Journal of Numerical Methods in Engineering* **47**: 2019–2037.
Horritt MS, Bates PD. 2001. Predicting floodplain inundation: raster-based modelling versus the finite element approach. *Hydrological Processes* **15**: 825–842.
Horritt MS Mason DC, Luckman AJ. 2001. Flood boundary delineation from synthetic aperture radar imagery using a statistical active contour model. *International Journal of Remote Sensing* **22**: 2489–2507.
Isaaks EH, Srivastava RM. 1989. *An Introduction to Applied Geostatistics*. Oxford University Press: Oxford, UK; 651 pp.
King IP, Roig L. 1988. Two dimensional finite element models for floodplains and tidal flats. In *Proceedings of an International Conference on Computational Methods in Flow Analysis*, Okayama, Japan, Niki K, Kawahara M (eds); 711–718.
Knupp P. 1995. Mesh generation using vector fields. *Journal of Computational Physics* **119**: 142–148.
Kouwen N. 2000. Closure of 'Effect of riparian vegetation on flow resistance and flood potential'. *Journal of Hydraulic Engineering, American Society of Civil Engineers* **126**: 954.
Kouwen N, Fathi-Maghadam M. 2000. Friction factors for coniferous trees along rivers. *Journal of Hydraulic Engineering, American Society of Civil Engineers* **126**: 732–740.
Kouwen N, Li RM. 1980. Biomechanics of vegetative channel linings. *Journal of the Hydraulic Division, American Society of Civil Engineers* **106**: 713–728.
Lee J. 1989. A drop heuristic method for extracting irregular networks for digital elevation models. In *Proceedings of GIS/LIS '89*, American Congress of Surveying and Mapping: Falls Church, USA; 30–39.
Lee J. 1991. Comparison of existing methods for building triangular irregular network models of terrain from grid digital elevation models. *International Journal of Geographical Information Systems* **5**: 267–285.
Löhner R. 2001. *Applied CFD Techniques: An Introduction Based on Finite Element Methods*. John Wiley and Sons: Chichester, UK; 366 pp.
Lynch DR, Gray WG. 1980. Finite element simulation of flow deforming regions. *Journal of Computational Physics* **36**: 135–153.
Marchuk GI. 1975. *Methods of Numerical Mathematics*. Springer-Verlag: New York; 316 pp.
Marks K, Bates PD. 2000. Integration of high resolution topographic data with floodplain flow models. *Hydrological Processes* **14**: 2109–2122.
Mason DC, Cobby DM, Horritt MS, Bates PD. Submitted. Floodplain friction parameterisation in two-dimensional river flood models using vegetation heights derived from airborne scanning laser altimetry. *Hydrological Processes*.
Nicholas AP, Walling DE. 1997. Modelling flood hydraulics and overbank deposition on river floodplains. *Earth Surface Processes and Landforms* **22**: 59–77.
Puppo E, Cignoni P, Montani C, Scopigno R. 1997. Multi-resolution representation and visualisation of volume data. *IEEE Transactions on Visualisation and Computer Graphics* **3**: 352–369.
Rebay S. 1994. Efficient unstructured mesh generation by means of Delaunay triangulation and Bowyer–Watson algorithm. *Journal of Computational Physics* **110**: 23–38.
Stewart M, Bates PD, Price D, Burt TP. 1998. Modelling contamination in floodplain soils. *Hydrological Processes* **12**: 1233–1266.
Temple DM. 1987. Closure of 'Velocity distribution coefficients for grass-lined channels'. *Journal of Hydraulic Engineering, American Society of Civil Engineers* **113**: 1224–1226.
Wood EF, Sivapalan M, Beven K, Band L. 1988. Effects of spatial variability and scale with implications for hydrological modelling. *Journal of Hydrology* **102**: 29–47.

